

Is there a redshift cutoff for submillimetre galaxies?

G. Raymond^{1*}, S. A. Eales¹, S. Dye¹, R. Carlberg² and M. Sullivan³

¹*Cardiff University, School of Physics & Astronomy, Queens Buildings, The Parade, Cardiff, CF24 3AA, U.K.*

²*Department of Astronomy and Astrophysics, University of Toronto, Toronto, ON M5S 3H4, Canada*

³*Department of Physics (Astrophysics), University of Oxford, Denys Wilkinson Building, Keble Road, Oxford, OX1 3RH, U.K.*

27-07-09

ABSTRACT

We present new optical and infrared photometry for a statistically complete sample of seven 1.1 mm selected sources with accurate coordinates. We determine photometric redshifts for four of the seven sources of 4.64, 4.54, 1.49 and 0.18. Of the other three sources two are undetected at optical wavelengths down to the limits of very deep Subaru and Canada-France-Hawaii Telescope images (~ 27 mag AB, i band) and the remaining source is obscured by a bright nearby galaxy. The sources with the highest redshifts are at higher redshifts than all but one of the ~ 200 sources taken from the largest recent 850 μm surveys, which may indicate that 1.1 mm surveys are more efficient at finding sources at very high redshifts than 850 μm surveys.

We investigate the evolution of the number density with redshift of our sample using a banded V_e/V_a analysis and find no evidence for a redshift cutoff, although the number of sources is very small. We also perform the same analysis on a statistically complete sample of 38 galaxies selected at 850 μm from the GOODS-N field and find evidence for a drop-off in the number density beyond $z \sim 1$ and 2, confirming the earlier conclusion of Wall, Pope & Scott (2008). We also find evidence for the existence of two differently evolving sub-populations separated in luminosity, with the drop-off in density for the low-luminosity sources occurring at a lower redshift.

Key words: galaxies:distances and redshifts, galaxies:evolution, galaxies:high-redshift, submillimetre, infrared:galaxies, galaxies:statistics

1 INTRODUCTION

Submillimetre (submm) galaxies (SMGs), first detected at 850 μm with the Submillimetre Common User Bolometer Array (SCUBA) (Holland et al. 1999), are a significant population of high redshift star forming galaxies (e.g., Hughes et al. 1998; Blain et al. 2002). They are believed to be dust enshrouded galaxies undergoing prodigious levels of star formation (e.g., Hughes et al. 1998; Eales et al. 1999) in which the optical/UV radiation emitted by the stars is absorbed by the dust and then re-emitted in the submm. Star formation rates in excess of 1000 $M_\odot\text{yr}^{-1}$ have been inferred (Scott et al. 2002), much higher than locally. The galaxies in these samples have been found to account for up to one tenth of the total far-infrared/submm energetic background (e.g., Dye et al. 2007) and many authors have argued that these galaxies are the progenitors for the elliptical galaxies we see in the local Universe (Eales et al. 1999; Scott et al. 2002; Dunne, Eales & Edmunds 2003). Thus understanding the nature of these sources is of great

importance for the understanding of galaxy formation and evolution as a whole.

Observations of SMGs at ~ 1 mm benefit from a negative K-correction out to high redshifts due the shape of their spectral energy distribution (SED). As the redshift of an SMG increases, the peak of its rest-frame SED moves toward the observed waveband, offsetting the dimming caused by the increasing luminosity distance. This fact accounts for the surprising ability of SCUBA to find large numbers of high-redshift galaxies.

The large amount of dust responsible for the strong submm emission gives rise to high levels of attenuation in the optical. This in conjunction with the poor angular resolution of single dish submm facilities makes the cross identification of SMGs at different wavelengths difficult. Moreover, even when an optical counterpart can be identified, the high levels of dust attenuation makes the determination of a spectroscopic redshift difficult. As such we are currently unable to determine spectroscopic redshifts for the majority of SMGs. The strong correlation between dust emission and radio emission which appears to hold true in both the low-redshift and high-redshift universe (Vlahakis, Eales & Dunne 2007)

* E-mail: gwenifer.raymond@astro.cf.ac.uk

has been useful for both identifying the counterparts and estimating redshifts. Due to the low surface density of radio sources on the sky, the probability of the radio counterpart being coincidental with the submm source by chance is small. Due to the high positional accuracy of radio observations, it is then possible to identify the optical counterpart and retrieve a spectroscopic redshift. It is also possible to estimate the redshift using the ratio of radio to submm flux (e.g., Hughes et al. 1998; Carilli & Yun 1999, 2000; Smail et al. 2000).

Chapman et al. (2005), using the Low Resolution Imaging Spectrograph (LRIS) (Oke et al. 1995) on the Keck I telescope, managed to obtain spectroscopic redshifts for a total of 73 radio-identified SMGs with a median 850 μm flux of 5.3 mJy. The galaxies in this sample were found to lie at a median redshift of $z = 2.2$ out to a maximum value of $z_{max} = 3.6$. However, the K-correction which allows us to detect high-redshift SMGs does not similarly benefit their radio fluxes and so radio identified SMGs are subjected to a radio selection effect which limits redshifts to $z \lesssim 3$.

Pope et al. (2006), produced the first complete (i.e. not requiring radio IDs) sample of 850 μm selected SMGs that has close to 100% redshifts. The sample consists of 35 galaxies, 21 with secure optical counterparts and 12 with tentative optical counterparts, and its completeness means that unlike previous surveys it is not biased towards low- z sources. The median redshift determined for this sample is $z \sim 2.2$. Using this sample, Wall, Pope & Scott (2008) examined the epoch dependency of the number density of SMGs. They found an apparent redshift cutoff at $z > 3$ with further evidence for two separately evolving populations, divided by luminosity. However this result was based on calculations using a single model galaxy SED. Since the predicted relationship between submm flux-density and redshift depends strongly on the assumed SED, one of the aims of this paper is to re-examine their conclusion using a range of empirical SEDs.

There have been a number of explanations for the lack of high-redshift SMGs. Given that dust is thought to form in the atmospheres of highly evolved stars, it is possible that at high redshifts simply not enough time has passed for dust to form (Morgan & Edmunds 2003). Observations of high-redshift quasars have however detected high levels of dust (e.g., Priddey & McMahon 2001), suggesting that this is not the explanation. Another possible explanation is that there are fewer large star-forming galaxies at high redshifts.

Eales et al. (2003) presented evidence that SMGs typically have low values for the ratio of the 850 μm to 1200 μm fluxes compared to that expected from a low redshift galaxy. One possible explanation is that these sources are at very high redshifts. If this is true, then observations at 1.1 mm would be better at detecting SMGs at the highest redshifts than observations at 850 μm . A new complete sample of 1.1 mm selected SMGs located in the COSMOS field (Scoville et al. 2007) has been compiled by Younger et al. (2007). The sources were selected initially at 1.1 mm with the AzTEC camera (Scott et al. 2008; Wilson et al. 2008) on the JCMT. The resultant catalogue consists of 44 sources with $S/N > 3.5\sigma$, 10 of which are robust with $S/N > 5\sigma$. Follow up observations by Younger et al. (2007) were then made with the Submillimetre Array (SMA) at 890 μm for the 7 highest significance AzTEC sources, allowing their po-

sitions to be determined with an accuracy of $\sim 0.2''$. The COSMOS field offers a wealth of data over a great number of wavebands including the optical and infrared. Thus the high positional accuracy allows for the identification of optical counterparts and hence the determination of photometric redshifts. Of the seven AzTEC sources imaged with the SMA six have IRAC counterparts, and one source is obscured by a nearby bright galaxy. Using deep Hubble Space Telescope (HST) imaging acquired with the Advanced Camera for Surveys (ACS), Koekemoer et al. (2007) found optical counterpart candidates for only three of these sources.

The main aim of this paper is to carry out a deeper search for the optical counterparts for the AzTEC sources. We give photometry from deep Subaru and Canada-France-Hawaii-Telescope (CFHT) imaging and find one new possible optical ID. We estimate photometric redshifts for the AzTEC sources using the HYPERZ photometric redshift package (Bolzonella, Miralles & Pelló 2000). Throughout this work we employ a concordance cosmological model with $\Omega_{total} = 1$, $\Omega_m = 0.3$, $\Omega_\Lambda = 0.7$ and $H_0 = 75 \text{ kms}^{-1}\text{Mpc}^{-1}$. All magnitudes quoted are AB.

2 NEW IMAGES AND PHOTOMETRY FOR THE AZTEC SAMPLE

We searched for optical counterparts and measured new photometry using deep Subaru¹, CFHT and IRAC images of the AzTEC sources. The IRAC and Subaru images are the publicly available COSMOS images taken by the COSMOS team (Scoville et al. 2007). The CFHT images are taken from the CFHT Deep Legacy Survey. The images we used were taken using the CFHT g_M, r_M, i_M, z_M , Subaru $B_j, V_j, r+, i+, z+$ and IRAC channel 1 and 2 filters to average 3σ depths of approximately 28.4, 27.9, 27.6, 26.5, 29.0, 28.2, 28.3, 27.7, 26.4, 24.1 and 23.6 mags respectively.

We searched the i-band images (figure 2) at the SMA coordinates. We find bright i-band counterparts for AzTEC1, 3 and 7, all of which were previously known. We also find a faint i-band counterpart for AzTEC5 at the SMA coordinates. We find no objects directly at the SMA coordinates for AzTEC2, but there is a bright object offset from this position by $3''$, meaning that the magnitude limits of this SMG are not useful.

We find no optical counterparts directly at the SMA coordinates for AzTEC4 and 6 in the Subaru and CFHT imaging. For the latter source, however, there is a bright i-band counterpart offset from the SMA position by $\sim 0.6''$ ($\sim 3\sigma$) which could be AzTEC6's counterpart or the true counterpart may be too faint to see. There is also a faint i-band source, offset from AzTEC4's SMA position by $\sim 0.8''$ ($\sim 4\sigma$), in the Subaru imaging. For these two sources we added the i band CFHT and Subaru images, inversely weighting the images by the square of the noise, in order to try and detect any very faint possible counterparts. The stacked i-band images for AzTEC4 and 6 are shown in figure 2. We still do not find counterparts at the SMA positions for AzTEC4 and 6

¹ An additional uncertainty of 0.3 mags in the Subaru B_j band magnitudes is taken into account in this photometry due to the possibility of a red leak or a shift in the blue cutoff of this filter.

and given the good coincidence between the SMA and optical positions for the other AzTEC sources we tentatively conclude that the true counterparts have not yet been detected.

The typical full-width half-maximum (FWHM) of the optical and IRAC channel 1 and 2 point spread functions (PSFs) are $\sim 0.8''$, $1.66''$ and $1.72''$ respectively. Magnitudes were determined manually by placing apertures onto the images, ensuring that the aperture was large enough to contain as much of the emission from the galaxy as possible without including any emission from neighboring objects. Thus the sizes of the optical apertures vary from source to source, although are constant for a given source. We used larger apertures for the IRAC sources due to the images having a larger PSF, but use the procedure outlined below to correct for this.

Due to the difference in the PSF between the optical and IRAC images as well as the difference in the aperture sizes, a small correction needed to be applied to the IRAC magnitudes before they could be used in conjunction with optical magnitudes to determine a photometric redshift. We corrected IRAC magnitudes by firstly fitting a 2D Gaussian to the IRAC source. We then scaled it to have the FWHM it would have had if observed with CFHT/Subaru. The flux was then computed using the scaled Gaussian and new aperture size. All the corrections applied in this work increase the IRAC magnitudes, and the more extended the source the greater the correction. Corrections range from 0.01 to 0.46 magnitudes.

The new photometry is summarized in table 1, and the details of the individual objects are discussed below.

2.1 Notes on Individual Objects

AzTEC1- *J095942.86+022938.2* AzTEC1 is the brightest submm source in the sample with fluxes of $F_{890\mu m} = 15.6 \pm 1.1$ mJy and $F_{1.1mm} = 10.7 \pm 1.3$ mJy. There is a bright i-band object located directly at the SMA position. Optical fluxes are measured using an aperture $1.94''$ in diameter and the source is detected in the Subaru i+ band at 25.11 ± 0.03 mag which is in agreement with the HST i-band magnitude given in Younger et al. (2007). There is some disagreement within the same wavebands between the CFHT and Subaru and photometry (table 1), but the discrepancy is small enough that the photometric redshift is not significantly affected. IRAC magnitudes were measured using an aperture of diameter $4.45''$. Only a small correction was applied to the IRAC magnitudes: $+0.01$ mag in both IRAC channel 1 and 2.

AzTEC2- *J100008.05+022612.2* AzTEC2 is detected in the submm with fluxes $F_{890\mu m} = (12.4 \pm 1.0)$ mJy and $F_{1.1mm} = (9.0 \pm 1.3)$ mJy. No objects are found directly at the SMA coordinates, but there is a bright object offset from SMA position by $3''$. Thus the limit on the magnitude of the optical counterpart is not very useful.

AzTEC3- *J100020.70+023520.5* AzTEC3 is detected in the submm with fluxes $F_{890\mu m} = 8.7 \pm 1.5$ mJy and $F_{1.1mm} = 7.6 \pm 1.2$ mJy. There is a bright i-band object located at the SMA coordinates as well as three companion objects offset by between $1''$ and $2''$. Since SMGs often

seem to consist of multiple components (Ivison et al. 1998) it is possible that these companion objects are also part of AzTEC3. However, since six of the seven AzTEC sources are detected in the IRAC bands, it seems likely that if the companion objects are part of the same galaxy then they should also be contributing to the IRAC emission. We attempted to determine whether this is the case by convolving the Subaru image with the IRAC beam and comparing the FWHM of the IRAC source with that of the convolved Subaru image. We find that the FWHM of the convolved image is $\sim 4.4''$. The FWHM of the IRAC $3.6 \mu m$ image is $\sim 2.87''$, suggesting that the $3.6 \mu m$ emission is associated only with the central object. Optical fluxes were measured using a aperture of diameter $1.26''$ and the source is detected in the Subaru i+ band at 26.18 ± 0.08 mag which is in agreement with the HST i-band magnitude. The CFHT and Subaru magnitudes within the same bands are consistent with each other. IRAC magnitudes were measured using an aperture of diameter $4.80''$. A correction of $+0.2$ mag was applied to the IRAC magnitudes in channels 1 and 2.

AzTEC4- *J095931.72+023044.0* AzTEC4 is detected in the submm with fluxes $F_{890\mu m} = 14.4 \pm 1.9$ mJy and $F_{1.1mm} = 6.8 \pm 1.3$ mJy. We find a tentative i-band counterpart, offset from the SMA position by $0.8''$ ($\sim 3\sigma$), in the Subaru image with a magnitude of 27.43 ± 0.13 . In the combined image (see above), the counterpart can be seen more clearly and has a magnitude of 26.99 ± 0.18 in a $2.57''$ diameter aperture. However we find it is too faint to detect in our other Subaru and CFHT bands. IRAC magnitudes were measured using an aperture of diameter $4.80''$. Corrections of $+0.11$ and $+0.04$ mags were applied to the IRAC magnitudes in channels 1 and 2 respectively. Because of the good agreement between the SMA the optical positions for the other AzTEC sources we tentatively conclude that this is not the true counterpart.

AzTEC5- *J100019.75+023204.4* AzTEC5 is detected in the submm with fluxes $F_{890\mu m} = 9.3 \pm 1.3$ mJy and $F_{1.1mm} = 7.6 \pm 1.3$ mJy. Younger et al. (2007) found no optical counterpart in ACS imaging, but we find a faint Subaru source at the SMA coordinates with a Subaru i+ band magnitude of 26.74 ± 0.13 , measured in an aperture of diameter $1.68''$. The CFHT and Subaru magnitudes within the same bands are consistent with each other. IRAC magnitudes were measured using a aperture of diameter $4.80''$. Corrections of $+0.46$ and $+0.14$ mag were applied to the IRAC magnitudes in channels 1 and 2 respectively.

AzTEC6- *J100006.50+023837.7* AzTEC6 is detected in the submm with fluxes $F_{890\mu m} = 8.6 \pm 1.3$ mJy and $F_{1.1mm} = 7.9 \pm 1.2$ mJy. Younger et al. (2007) find no optical counterpart in ACS imaging. In CFHT and Subaru imaging we find no source directly at the SMA coordinates, but we do find a source offset from the SMA position by $\sim 0.6''$ ($\sim 3\sigma$). This could therefore be the optical counterpart, or the true counterpart may be too faint to detect. The source offset from the SMA position has a Subaru i+ magnitude of 25.38 ± 0.04 magnitudes, measured in an aperture of diameter $1.59''$. The CFHT and Subaru magnitudes within the same bands are consistent with each

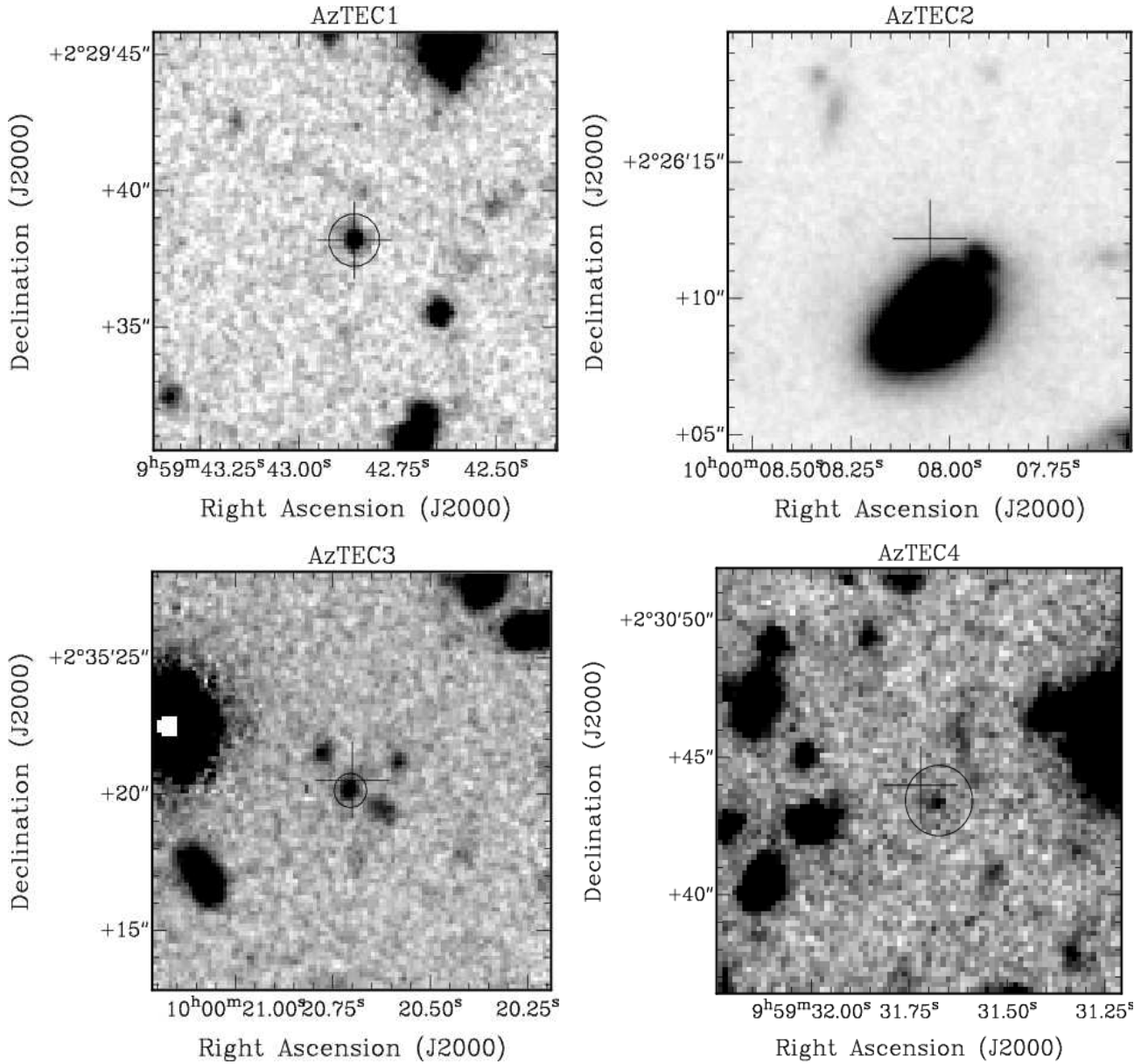


Figure 1. Subaru $i+$ band cutouts for AzTEC1 to 7, with the exception of AzTEC4 and 6, which are the combined CFHT and Subaru i -band images. Each image has a field of view of $15.3'' \times 15.3''$ and a scale of $0.15''/\text{pixel}$. The SMA coordinates of each source are highlighted by cross-hairs and the optical counterpart (including the objects offset from AzTEC4' and 6s SMA coordinates by $\sim 0.8''$ and $\sim 0.6''$ respectively, see text) is circled with an aperture the size of which was used in its photometry. SMA coordinates are accurate to $\sim 0.2''$.

other. IRAC magnitudes were measured using an aperture of diameter $5.88''$. A correction of $+0.13$ mag is applied to the IRAC magnitudes in channels 1 and 2. Because of the good agreement between the SMA the optical positions for the other AzTEC sources we tentatively conclude that this is not the true counterpart, although we do estimate a photometric redshift for it.

AzTEC7- $J100018.06+024830.5$ AzTEC7 is detected in the submm with fluxes $F_{890\mu\text{m}} = 12.0 \pm 1.5$ mJy and $F_{1.1\text{mm}} = 8.3 \pm 1.4$ mJy. We find an optical counterpart with a disturbed morphology at the SMA coordinates which could be a system of merging galaxies. Optical fluxes were

measured by placing an aperture of diameter $2.87''$ over the whole of the system. The source is detected in the Subaru $i+$ band at 24.20 ± 0.04 mag. IRAC magnitudes were measured using an aperture of diameter $6.12''$. Corrections of $+0.08$ and $+0.02$ mag were applied to the IRAC magnitudes in channels 1 and 2 respectively.

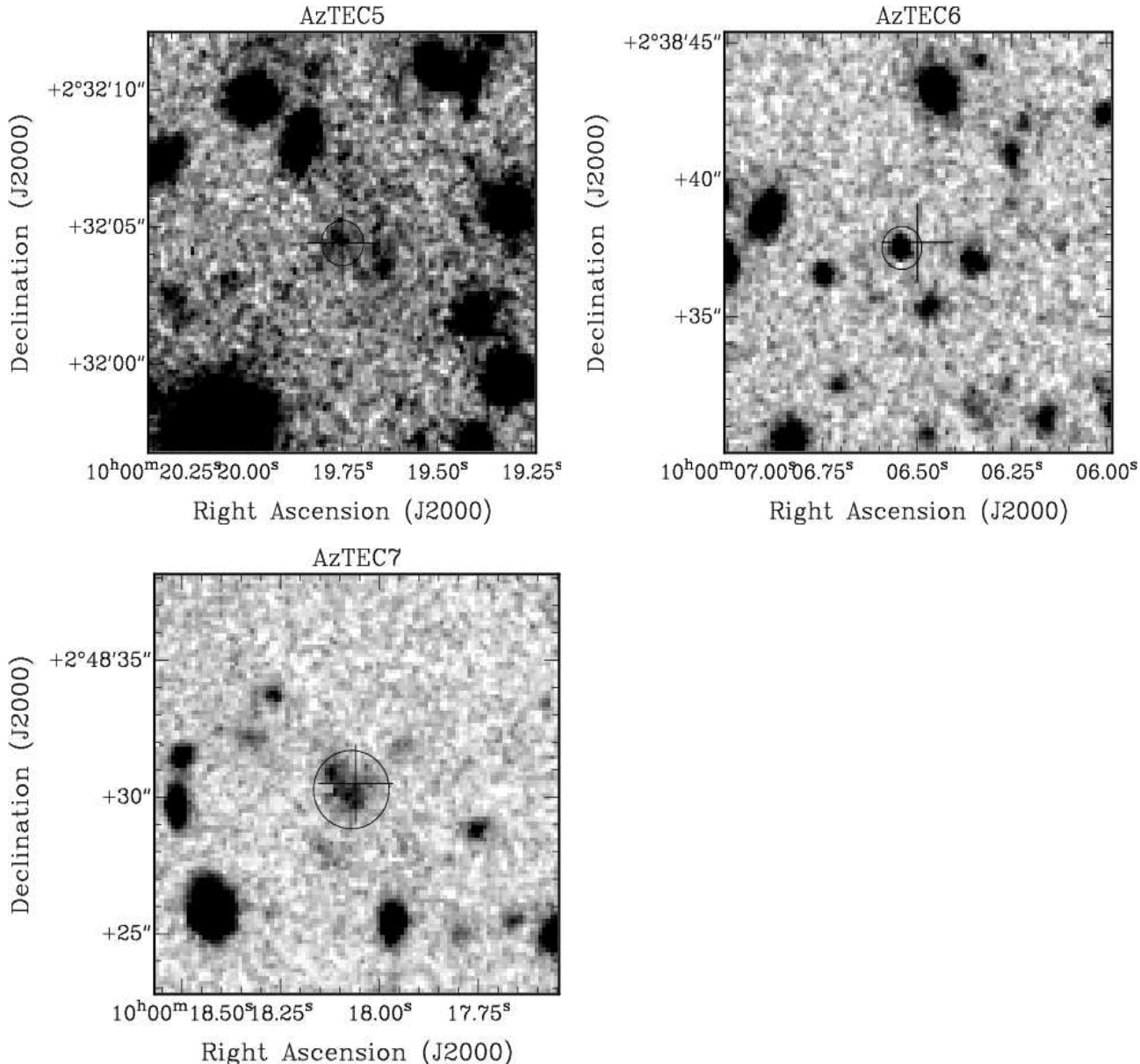


Figure 1 – continued

3 ESTIMATED REDSHIFTS FOR THE AZTEC SAMPLE

Photometric redshifts were determined by applying the photometric redshift package, HYPERZ (Bolzonella, Miralles & Pelló 2000), to our 11 band photometry (Subaru: B, V, r+, i+, z+; CFHT: g_M , r_M , i_M , z_M ; IRAC: 3.6 μm , 4.5 μm). The spectra used for fitting in this work are taken from the set compiled by Dye et al. (2008), which is optimized for the determination of photometric redshifts when including filters in the near/mid-infrared. Dye et al. (2008) compared the photometric redshifts determined using these spectral templates with those determined using synthetic spectra constructed from the best-fit star formation history for their sample of 60 SCUBA sources. Since these methods are completely independent and the redshifts found using both sets of

templates were found to be in good agreement, we assume that our template set is adequate.

We varied the redshift in the range $z = 0$ to 10. We employed the reddening regime of Calzetti et al. (2000), with A_V allowed to vary in the range $A_V = 0$ to 5 in steps of 0.2. We used a minimum photometric error of 0.05 magnitudes for each band. For wavebands in which we have no detection we took the flux of the source to be zero with a 1σ error equal to the sensitivity of the detector in that waveband. The photometric redshifts obtained are listed in table 2.

The median redshift of the sample is 2.7 which is somewhat higher than the median redshift, 2.2, of the sample presented by Chapman et al. (2005). The maximum redshift found is 4.64 and the minimum redshift found is 0.18. Comparing the redshift distribution of this sample to that of the samples presented in Chapman et al. (2005), Pope et al.

	AzTEC1	AzTEC2	AzTEC3	AzTEC4	AzTEC5	AzTEC6	AzTEC 7
RA	09:59:42.86	10:00:08.05	10:00:20.70	09:59:31.72	10:00:19.75	10:00:06.50	10:00:18.06
Dec	+02:29:38.2	+02:26:12.2	+02:35:20.5	+02:30:44.0	+02:32:04.4	+02:38:37.7	+02:48:30.5
Optical Ap. Size	1.94"	...	1.26"	2.57"	1.68"	...(1.59")	2.87"
m_B	>28.88	...	>29.14	>28.67	28.80±0.47	>28.98(25.80±0.30)	25.67±0.31
m_V	27.13±0.17	...	28.77±0.75	>28.21	28.76±0.62	>28.32(25.67±0.04)	25.10±0.06
m_{r+}	26.21±0.06	...	27.39±0.22	>28.02	27.07±0.13	>28.47(25.77±0.03)	24.97±0.05
m_{i+}	25.11±0.03	...	26.18±0.08	(27.43±0.13)	26.74±0.13	>27.97(25.38±0.04)	24.20±0.04
m_{z+}	25.02±0.02	...	25.58±0.15	>26.50	26.07±0.22	>26.79(24.80±0.06)	23.65±0.07
g_M	>28.12	...	>28.71	>27.93	>28.41	>28.42(26.16±0.05)	N/A
r_M	26.54±0.15	...	27.13±0.24	>27.46	27.15±0.20	>27.96(25.61±0.05)	N/A
i_M	25.25±0.05	...	26.30±0.12	>26.19	26.50±0.13	>27.81(25.42±0.05)	N/A
z_M	25.11±0.13	...	25.69±0.22	>26.27	26.46±0.38	>26.06(24.87±0.08)	N/A
IRAC Ap. Size	4.45"	...	4.80"	4.80"	4.80"	5.88"	6.12"
$m_{3.6\mu m}$	23.40±0.07	...	23.72±0.11	22.11±0.04	23.24±0.08	24.13±0.25	20.63±0.01
$m_{4.5\mu m}$	23.08±0.08	...	22.98±0.12	22.15±0.04	22.31±0.06	23.50±0.27	20.15±0.02

Table 1. Photometry for the AzTEC sources, given in AB magnitudes. First two rows give the SMA co-ordinates. Aperture sizes are the diameters used for measuring optical and IRAC magnitudes. The IRAC magnitudes are corrected to take into account the difference in the seeing and aperture sizes for the IRAC and optical imaging (see text). No optical counterparts were found for AzTEC2. The only nearby optical counterparts for AzTEC4 and 6 are offset from their SMA positions by $\sim 4\sigma$ and $\sim 3\sigma$ respectively. We give the photometry for these objects in parentheses.

ID	z	χ_{min}^2	Notes
AzTEC1	4.64 ± 0.06	1.537	...
AzTEC2	No optical counterpart.
AzTEC3	4.54 ± 0.10	2.196	There is a secondary chi-squared minimum at the lower redshift of $z \sim 0.4$ with a chi-squared fit value of ~ 3.5 .
AzTEC4	Nearest counterpart only detected in one optical band.
AzTEC5	1.49 ± 0.10	1.488	There is a secondary chi-squared minimum at the higher redshift of $z \sim 4$ with a chi-squared fit value of ~ 4 .
AzTEC6	(2.09 ± 0.01)	(6.172)	The redshift and chi-squared values are for the optical source offset from AzTEC6's SMA position. The chi-squared fit to this source is much poorer compared to the others in the sample. This may further imply that the nearby optical counterpart we have selected is not the true counterpart to AzTEC6 and that the IRAC emission is unassociated with the optical emission.
AzTEC7	0.18 ± 0.01	7.021	CFHT data not available. There are several other possible redshifts with chi-squared fit values of ~ 10 up to $z \sim 2$. Even the best chi-squared fit is still relatively poor however, which may be due to the unusual nature of the source.

Table 2. The best photometric redshift fits for the sources with their minimum reduced χ^2 value, χ_{min}^2 . Notes of interest on the photometric redshifts, including secondary fits, for each source are also given. We do not give the best fit SED type as typically for each source there are several SED types which fit equally well. Note that reduced chi-squared values given here are not those directly output by HYPERZ, which takes the number of degrees of freedom as being the (number of filters−1). This is true if only the redshift is allowed to vary. However, we are additionally allowing A_v , SEDs type and the normalization to vary. Thus the correct number of degrees of freedom is given by (number of filters−4).

(2006), Dye et al. (2008) and Clements et al. (2008), we note that only one of the sources in this combined sample of ~ 200 850 μm selected sources is at a comparably high redshift as our two highest redshift sources, although this difference is not significant when analyzed with a Kolmogorov-Smirnov test. However two of the other AzTEC sources are undetected to very faint limits in the i-band, and these facts may indicate that 1.1 mm surveys find more sources at very high redshifts than 850 μm surveys.

4 A BANDED V_E/V_A ANALYSIS

Wall, Pope & Scott (2008) examined a sample of 38 SMGs

in the GOODS-N field and found evidence for a diminution in the space density of SMGs at redshifts $z > 3$. They also found evidence for two separately evolving sub-populations separated by luminosity. In this paper we present the results of our re-examination of this result using a banded V_e/V_a analysis and a range of empirical SEDs rather than the theoretical SED used by Wall et al.

The most well known method of investigating the evolution of the space density of galaxies with redshift is the $\langle V/V_{max} \rangle$ test (Schmidt 1968; Rowan-Robinson 1968). V is the co-moving volume enclosed by the galaxy (that volume which the field of view traces out in moving from a redshift of $z = 0$ out to the galaxy) and V_{max} is the volume that would be enclosed by the galaxy were it pushed

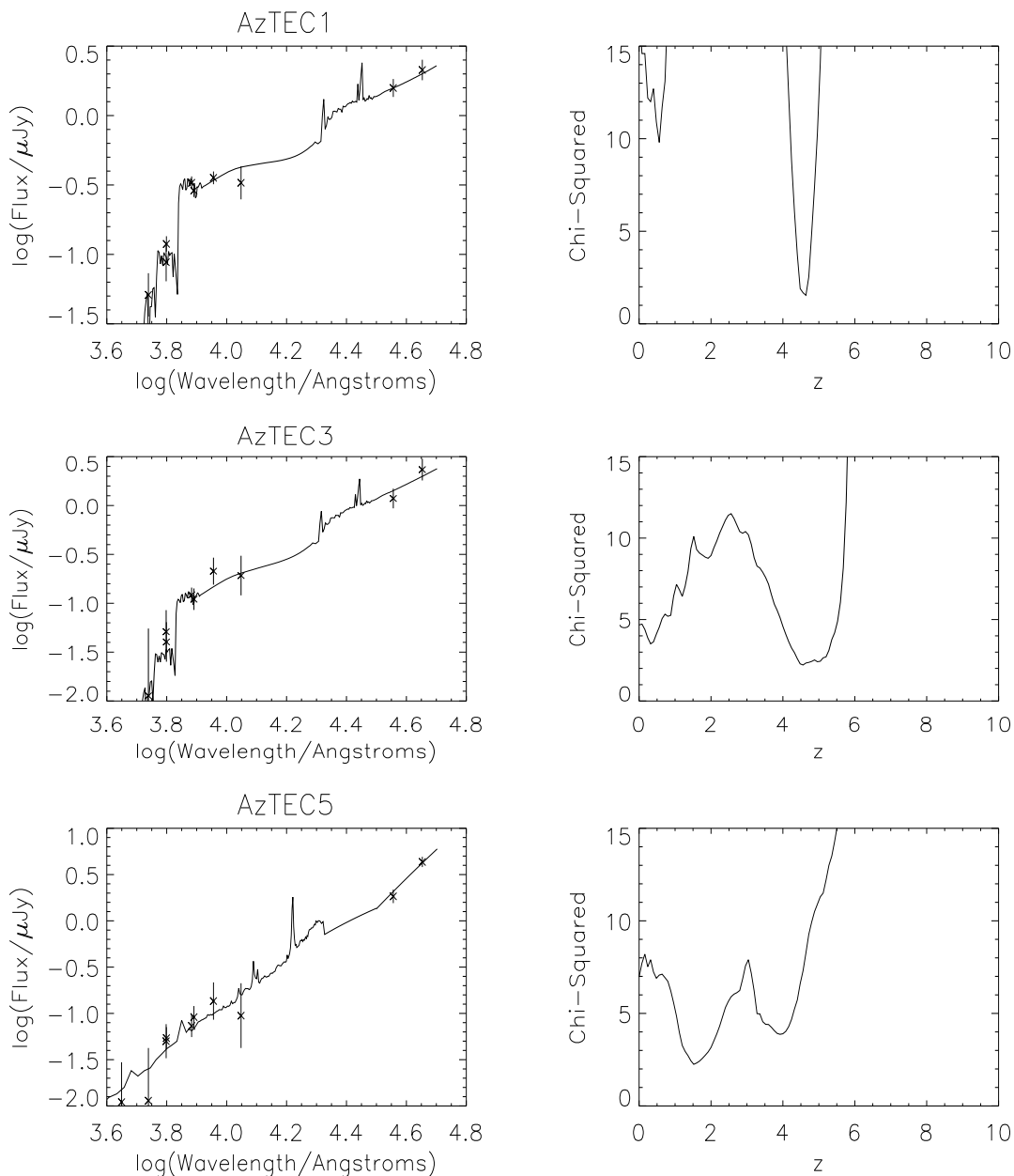


Figure 2. The left hand column shows the photometric data points for the AzTEC sources with optical counterparts. The best spectral fits for the sources are overlaid. The right hand column shows the marginalized reduced χ^2 distribution as a function of redshift. The AzTEC6 plots correspond to the nearby optically bright object.

to the redshift at which its flux drops to the survey limit. This method encounters problems when a survey encloses two galaxy populations, one undergoing positive evolution, and the other negative. If we have a uniform distribution of galaxies in space, then we expect the value of $\langle V/V_{max} \rangle$ to be $0.5 \pm (12N)^{-0.5}$, where N is the number of sources in the sample. A value of $\langle V/V_{max} \rangle > 0.5$ then implies a concentration of sources toward the more distant regions of their accessible volume and a value of $\langle V/V_{max} \rangle < 0.5$ implies a deficit of sources at higher redshifts. Therefore if we have in our sample separate populations undergoing high levels of positive and negative evolution, then $\langle V/V_{max} \rangle$ may still be close to 0.5, incorrectly implying zero evolution.

This problem can be solved by implementing instead a $\langle V_e/V_a \rangle$ test (Dunlop & Peacock 1990). This is effectively a banded version of the $\langle V/V_{max} \rangle$ test. V_e , the effective volume, is the volume enclosed between a minimum redshift z_{low} and the redshift of the galaxy. V_a , the accessible volume, is the volume enclosed between z_{low} and the redshift at which the galaxy's flux drops below the sensitivity of the survey. By investigating the variation of $\langle V_e/V_a \rangle$ with z_{low} we can distinguish between a positively evolving and a negatively evolving population.

We investigated the evolution of the space density of the sample with redshift through the implementation of a $\langle V_e/V_a \rangle$ test. Wall et al. based the k-correction necessary

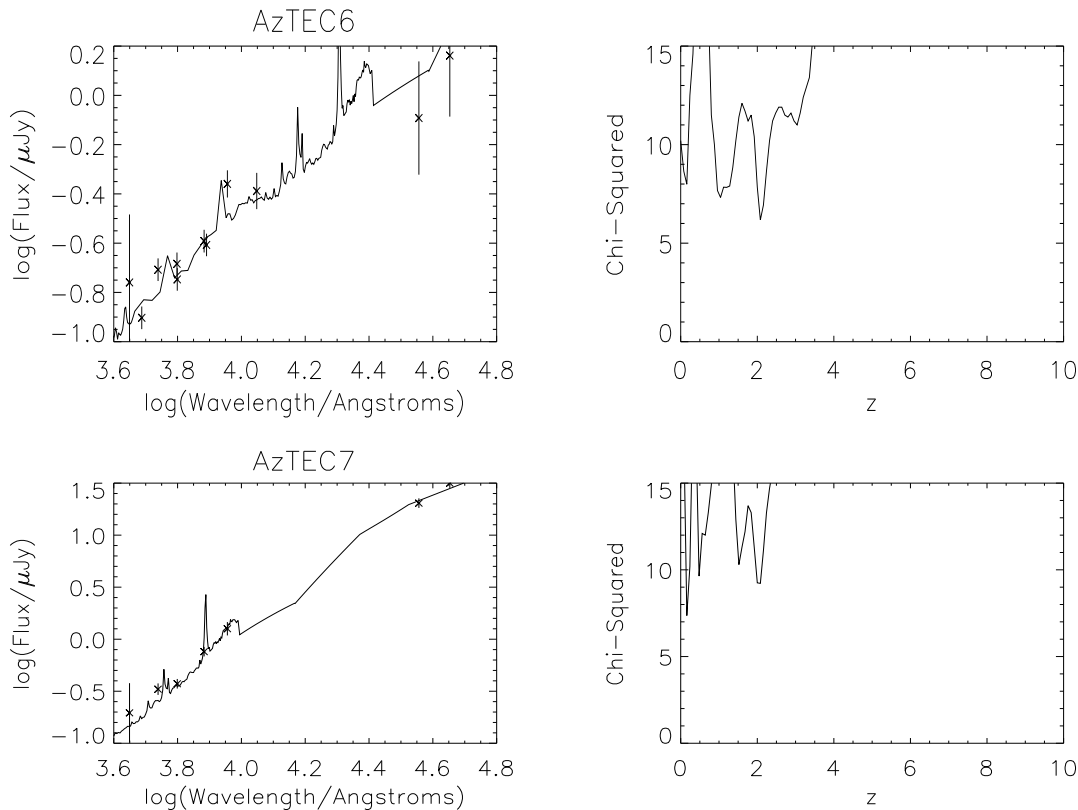


Figure 2 – continued

to calculate accessible volume on a single theoretical SED, whereas real galaxies have a range of SEDs. To investigate this, we carried out the $\langle V_e/V_a \rangle$ analysis using two different assumptions about SEDs. We used the two extreme two-component dust models of Dunne & Eales (2001), who provided fits to the hottest and coldest local SMGs. The cold SED, based on NGC 958, contains dust at temperatures of 20 and 44 K with a cold-to-hot dust mass ratio of 186:1. The hot SED, based on IR1525+36, contains dust at temperatures of 19 and 45 K with a cold-to-hot dust mass ratio of 15:1. Figure 3, which shows the predicted flux versus redshift plot for the different models, shows the effect of using different SED templates on the flux-redshift relation. The two SED types are normalized such that they produce a flux of 1 mJy at a redshift of $z = 1$.

We took the limiting flux of each source in the GOODS sample to be 3.5σ and measured $\langle V_e/V_a \rangle$ for $z_{low} = 0$ to 4 in steps of 0.1. We also separated sources into two samples of equal size according to luminosity. In doing this we are able to determine whether there are differences in the evolution of the two sub-populations.

Our results for the 38 SMGs of Wall, Pope & Scott are shown in figure 4. We find good evidence for the existence of a redshift cutoff at $z > 1$ for the hot SED, and slightly weaker evidence for a redshift cutoff at $z > 2$ for the cold SED. Dividing the sample into separate populations of high and low luminosity sources shows differences in the evolution of the two populations. The low luminosity sources show much sharper redshift cutoffs whereas the evidence for redshift cutoffs in the high luminosity sources

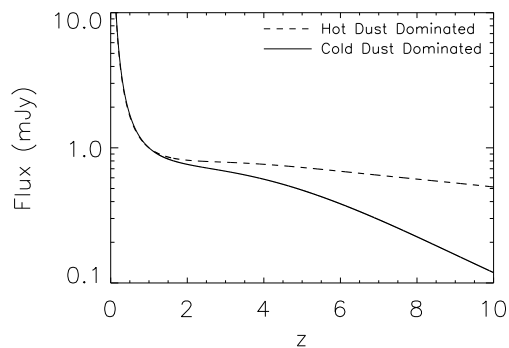


Figure 3. Flux versus redshift for both the cold (solid line) and hot (dashed line) SEDs. Both SEDs are normalized such that they produce a flux of 1 mJy at a redshift of $z = 1$.

is far more marginal. Thus we find evidence to support the conclusions given in Wall, Pope & Scott (2008): there is a redshift cutoff for the sample and that there is evidence for two separately evolving sub-populations

An additional uncertainty about this results is that Pope et al. (2006) claim that only 60% of their identifications are reliable. Therefore we also performed the $\langle V_e/V_a \rangle$ analysis only on sources with reliable identifications, the results of which are shown in figure 5. Using these sources only, we still find good evidence for a redshift cutoff at $z > 1$ for the hot SED, and some marginal evidence for a cutoff at

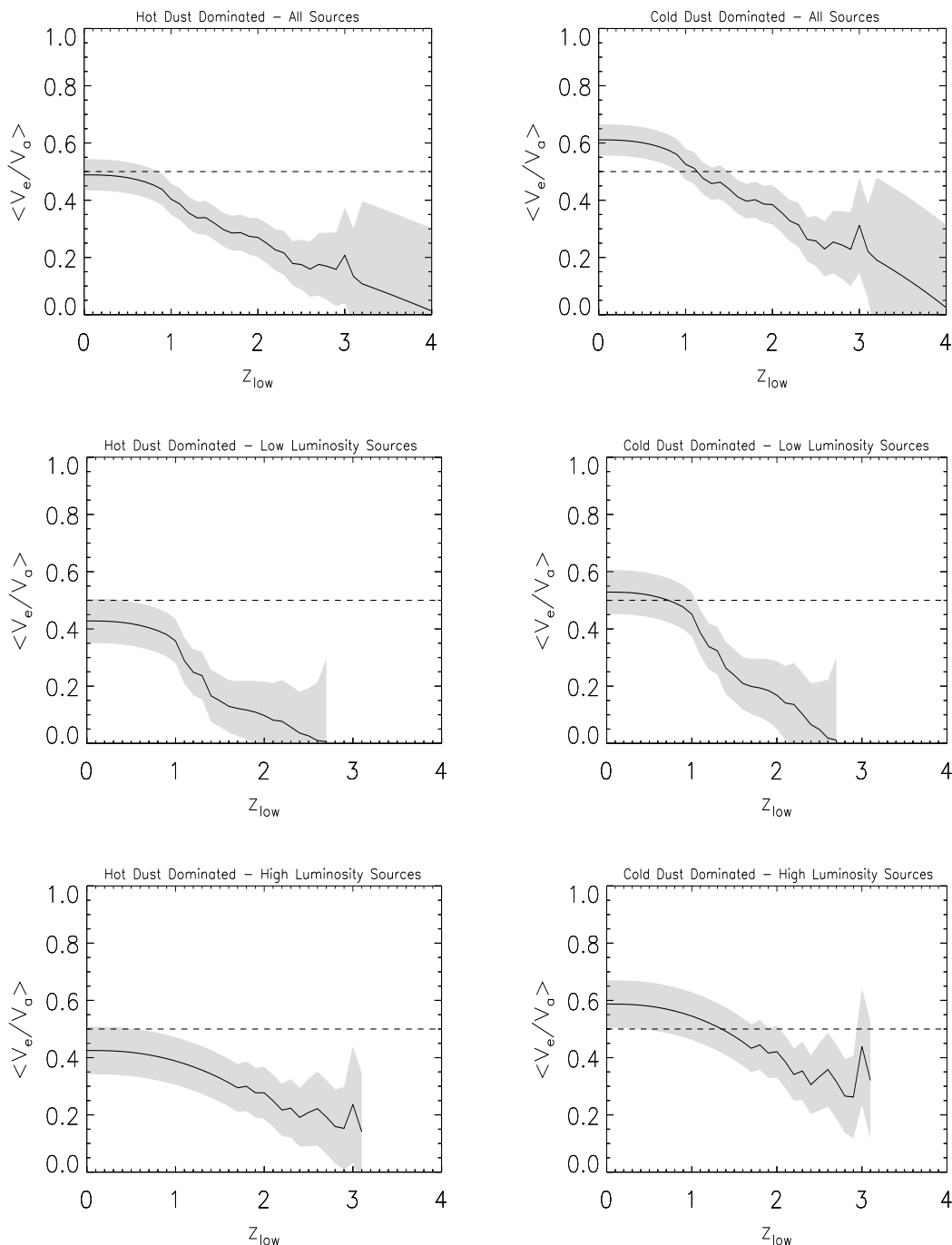


Figure 4. The distribution of the values of $\langle V_e/V_a \rangle$ with z_{low} for the GOODS-N sample. Figures in the left hand column are for hot SEDs and figures in the right hand column are for cold SEDs. The sample is also separated into high and low luminosity sources. The dashed line denotes the position of $\langle V_e/V_a \rangle = 0.5$ on the graph, values above which imply a concentration of galaxies at higher redshifts and below which imply a concentration of galaxies at lower redshifts. The grey shaded region shows the area enclosed by the 1σ error.

$z > 2$ for the cold SED. However, we are unable to find any clear evidence for two separately evolving galaxy subpopulations, separated in luminosity, as the sample size is too small.

However, by only taking into account the reliable identifications, we are probably biased towards optically brighter galaxies and therefore lower redshifts. We further investi-

gated the effect of the unreliable identifications by putting four (roughly half) of the unreliable identifications at $z = 4$ and repeating the analysis (figure 6). Doing this, we find that for hot SEDs our results are largely unaffected, with a relatively clear cutoff at redshifts higher than $z = 1$. However for the cold SEDs we find that our results are strongly affected, with no clear redshift cutoff up to a redshift of $z \sim 3$.

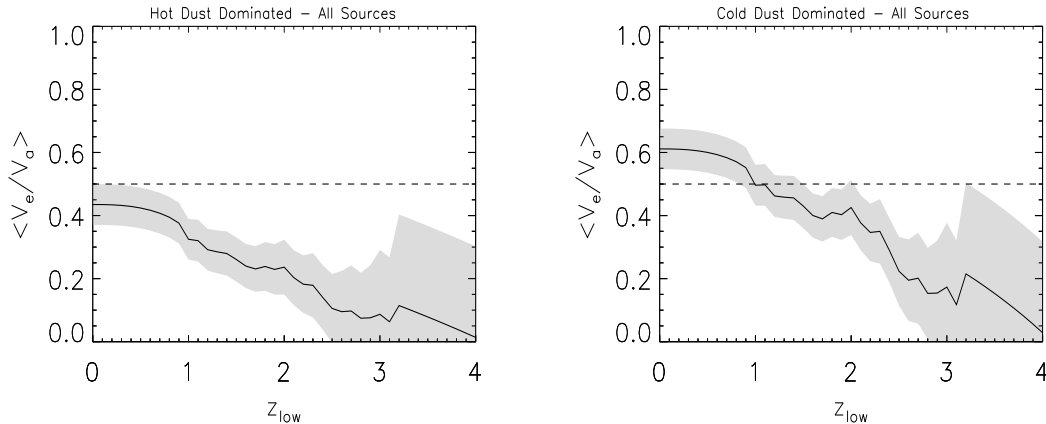


Figure 5. The distribution of the values of $\langle V_e/V_a \rangle$ with z_{low} for the GOODS-N sample, using only the sources with reliable identifications. Figures in the left hand column are for hot SEDs and figures in the right hand column are for cold SEDs. The dashed line denotes the position of $\langle V_e/V_a \rangle = 0.5$ on the graph, values above which imply a concentration of galaxies at higher redshifts and below which imply a concentration of galaxies at lower redshifts. The grey shaded region shows the area enclosed by the 1σ error.

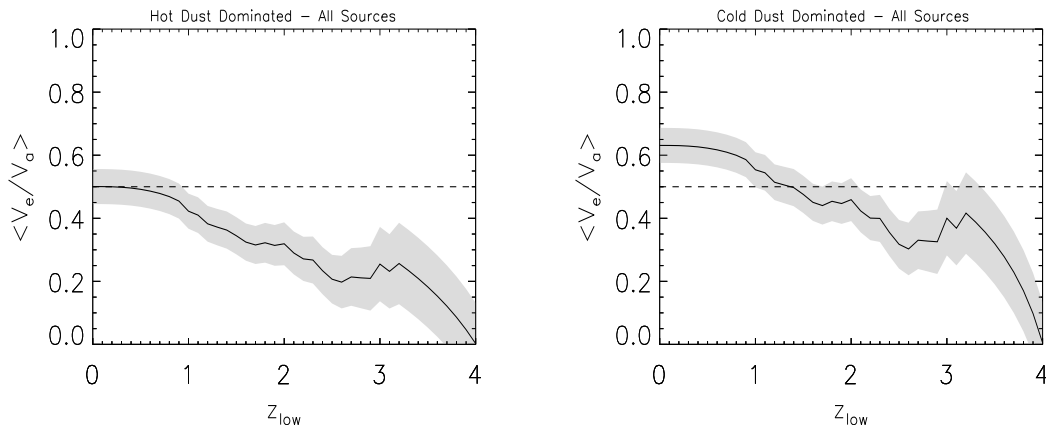


Figure 6. The distribution of the values of $\langle V_e/V_a \rangle$ with z_{low} for the GOODS-N sample, where four (roughly half) of the unreliable identifications have been pushed to redshifts of $z = 4$. Figures in the left hand column are for hot SEDs and figures in the right hand column are for cold SEDs. The dashed line denotes the position of $\langle V_e/V_a \rangle = 0.5$ on the graph, values above which imply a concentration of galaxies at higher redshifts and below which imply a concentration of galaxies at lower redshifts. The grey shaded region shows the area enclosed by the 1σ error.

We also performed a banded $\langle V_e/V_a \rangle$ analysis on our sample of AzTEC sources (excluding the AzTEC6 counterpart) the results of which are shown in figure 7, but our sample is too small to find any clear evidence of a redshift cutoff.

5 CONCLUSIONS

We give new Subaru, CFHT and IRAC photometry for a number of sources in the AzTEC / COSMOS survey with accurate coordinates from SMA imaging. We have estimated photometric redshifts for four of the seven galaxies in the sample. We find a median redshift of $z_{mean} \sim 2.57$ and a maximum of $z_{max} = 4.50$. Of the sources in the combined $850 \mu\text{m}$ surveys presented in Chapman et al. (2005), Pope et al. (2006), Dye et al. (2008) and Clements et al.

(2008), consisting of ~ 200 sources, only one is at a redshift greater than our two highest redshift sources. This in addition to the fact that we are unable to detect two of our sources in the optical bands down to very faint magnitudes may indicate that 1.1 mm surveys are more efficient at detecting very high-redshift sources than $850 \mu\text{m}$ surveys.

Re-investigating the space density evolution of a sample of 38 GOODS-N sources (Pope et al. 2006; Wall, Pope & Scott 2008) with more realistic SEDs we find a redshift cutoff at $z \sim 1$ if we assume a 'hot' SED and marginal evidence for a cutoff at $z \sim 2$ if we assume a 'cold' SED (in reasonable agreement with Wall et al.). Similar to Wall, Pope & Scott (2008) we also found evidence for two differently evolving sub-populations of SMGs, separated in luminosity, with high luminosity sources showing a less negative evolution.

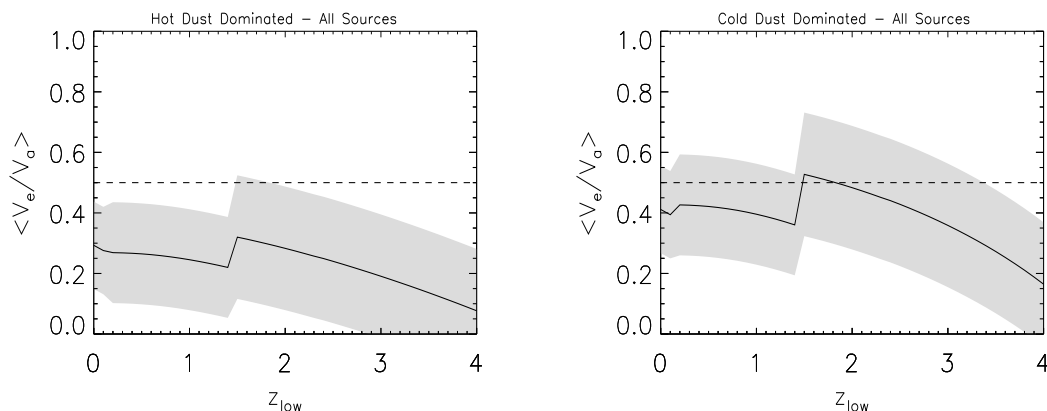


Figure 7. The distribution of the values of $\langle V_e/V_a \rangle$ with z_{low} for the AzTEC sample. The panels on the left hand side uses the hot SED and the panels on the right hand side uses the cold SED. The dashed line denotes the position of $\langle V_e/V_a \rangle = 0.5$ on the graph, values above which imply a concentration of galaxies at higher redshifts and below which imply a concentration of galaxies at lower redshifts. The grey shaded region shows the area enclosed by the 1σ error.

We performed a similar test on the AzTEC sources but were unable to draw any reliable conclusions as the sample is too small. The GOODS-N sample is also relatively small, and therefore any evidence for redshift cutoffs and differently evolving sub-populations must be treated with caution. In order to harden our conclusions in general we require larger surveys with accurate redshifts. We would also need surveys taken over larger areas of sky in order to take into account the effects of cosmic variance. Future, larger surveys (e.g. with Herschel, SCUBA2) therefore will enable us to more robustly determine the nature of the number density evolution of SMGs in the Universe.

Acknowledgements

G. Raymond, S. Eales and S. Dye acknowledge support from the Science and Technologies Facilities Council.

Based on observations obtained with MegaPrime/MegaCam, a joint project of CFHT and CEA/DAPNIA, at the Canada-France-Hawaii Telescope (CFHT) which is operated by the National Research Council (NRC) of Canada, the Institut National des Science de l'Univers of the Centre National de la Recherche Scientifique (CNRS) of France, and the University of Hawaii. This work is based in part on data products produced at TERAPIX and the Canadian Astronomy Data Centre as part of the Canada-France-Hawaii Telescope Legacy Survey, a collaborative project of NRC and CNRS.

REFERENCES

Blain, A. W., Smail, I., Ivison, R. J., Kneib, J.-P., Frayer, D. T., 2002, *PhR*, 369, 111
 Bolzonella, M., Miralles, J.-M., Pelló, R., 2000, *A&A*, 363, 476
 Calzetti, D., Armus, L., Bohlin, R. C., Kinney, A. L., Koornneef, J., Storchi-Bergmann, T., 2000, *ApJ*, 533, 682
 Carilli, C. L., Yun, M. S., 1999, *ApJ*, 513, L13
 Carilli, C. L., Yun, M. S., 2000, *ApJ*, 530, 618

Chapman, S. C., Blain, A. W., Smail, I., Ivison, R. J., 2005, *ApJ*, 622, 772
 Clements et al., 2008, *MNRAS*, 387, 247
 Dunlop, J. S., Peacock, J. A., 1990, *MNRAS*, 247, 19+
 Dunne, L., Eales, S. A., 2001, *MNRAS*, 327, 697
 Dunne, L., Eales, S. A., Edmunds, M. G., 2003, *MNRAS*, 341, 589
 Dye, S., Eales, S. A., Ashby, M. L. N., Huang, J.-S., Egami, E., Brodwin, M., Lilly, S., Webb, T., 2007, *MNRAS*, 375, 725
 Dye, S., et al., 2008, *MNRAS*, 386, 1107
 Eales, S. A., Lilly, S., Gear, W., Dunne, L., Bond, J. R., Hammer, F., Le Fèvre, O., Crampton, D., 1999, *ApJ*, 515, 518
 Eales, S., Bertoldi, F., Ivison, R., Carilli, C., Dunne, L., Owen, F., 2003, *MNRAS*, 344, 169
 Holland, W. S., et al., 1999, *MNRAS*, 303, 659
 Hughes, D. H., et al., 1998, *Nature*, 394, 241
 Ivison, R. J., Smail, I., Le Borgne, J.-F., Blain, A. W., Kneib, J.-P., Bezecourt, J., Kerr, T. H., Davies, J. K., 1998, *MNRAS*, 298, 583
 Koekemoer et al., 2007, *ApJ supplemental*, 172, 196
 Morgan, H. L., Edmunds, M. G., 2003, *MNRAS*, 343, 427
 Oke, J. B., et al., 1995, *PASP*, 107, 375+
 Pope et al., 2006, *MNRAS*, 370, 1185
 Priddey, R. S., McMahon, R. G., 2001, *MNRAS*, 342, L17
 Rowan-Robinson, M., 1968, *MNRAS*, 138, 445+
 Schmidt, M., 1968, *ApJ*, 151, 393+
 Scott, S. E., 2002, *MNRAS*, 331, 817
 Scott, K. S. et al., 2008, *MNRAS*, 385, 2225
 Scoville, N., et al., 2007, *ApJ supplemental*, 172, 150
 Smail, I., Ivison, T. J., Owen, F. N., Blain, A. W., 2000, *ApJ*, 528, 612
 Vlahakis, C., Eales, S., Dunne, L., 2007, *MNRAS*, 379, 1042
 Wall, J. V., Pope, A., Scott, D., 2008, *MNRAS*, 383, 435
 Younger, J. D., et al., 2007, *ApJ*, 671, 1531
 Wilson, G. W., et al., 2008, *MNRAS*, 386, 807